JOURNAL OF AIRCRAFT
Vol. 47, No. 2, March–April 2010

Effects of Unsteady Trailing-Edge Blowing on Delta Wing Aerodynamics

Ping Jiang,* Zhijin Wang,† and Ismet Gursul‡
University of Bath, Bath, England BA2 7AY, United Kingdom

DOI: 10.2514/1.45890

The effects of unsteady trailing-edge blowing on delta wing aerodynamics were investigated experimentally to understand the aerodynamics–propulsion interaction for dynamic thrust vectoring. Two models with sweep angles of $\Lambda = 50$ and 65 deg, representing nonslender and slender delta wings, respectively, were tested in a water tunnel. Flow visualization and velocity and force measurements were conducted at stall and poststall incidences. For the periodic blowing, it was found that the dynamic response of leading-edge vortex breakdown and wing normal force coefficient exhibit phase lags for both nonslender and slender delta wings. The estimated time constants are larger than those reported in the literature for unsteady wings undergoing pitching or plunging. In the case of transient blowing, the time delay for the decelerating jet is significantly larger than that for the accelerating jet. The variation of the circulation and the reattachment process near the wing surface were studied by means of velocity measurements. The range of the estimated time constants is similar at the stall and poststall incidences for both the slender and nonslender wings.

Nomenclature

A_{jet}	=	cross-sectional area of nozzle exit
b	=	wing span
C_N	=	normal force coefficient
C_μ	=	jet momentum coefficient, $\rho U_{\text{jet}}^2 A_{\text{jet}} / \frac{1}{2}\rho U_\infty^2 S_w$
c	=	chord length
f	=	frequency
f^*	=	dimensionless frequency, fc/U_∞
q	=	freestream dynamic pressure
Re	=	Reynolds number
S_w	=	wing surface area
s	=	local semispan
T	=	period
t	=	wing thickness or time
U_{jet}	=	jet velocity
U_∞	=	freestream velocity
u	=	velocity
X_{bd}	=	distance from wing apex to leading-edge vortex breakdown location
y_{jet}	=	spanwise location of jet
α	=	wing incidence
β	=	jet pitch angle
Γ	=	circulation
ΔX_{bd}	=	peak-to-peak amplitude of the variation of the vortex breakdown location
Λ	=	leading-edge sweep angle
ν	=	fluid kinematic viscosity
ρ	=	air density
τ	=	time constant
ϕ	=	phase lag
ω	=	angular frequency
ω_x	=	streamwise vorticity

Received 8 June 2009; revision received 24 September 2009; accepted for publication 25 September 2009.

*Graduate Student, Department of Mechanical Engineering.
†Research Councils United Kingdom Academic Fellow, Department of Mechanical Engineering.
‡Professor, Department of Mechanical Engineering. Associate Fellow AIAA.

I. Introduction

AT HIGH angles of attack, delta wings can generate high lift, with better stability and control characteristics [1–3]. For this reason, current and future unmanned combat air vehicle (UCAV) designs have blended delta wing–body configurations. However, it was found that serious aerodynamic, stability, and control issues exist for these configurations due to the absence of conventional aerodynamic control surfaces, such as the fin and tailplane [4,5]. Therefore, there is a need to explore and understand alternative methods of providing sufficient levels of stability and control for these tailless designs. Trailing-edge thrust-vectoring control has been widely regarded as an effective technology for improving the maneuverability and stability of future unmanned aircraft.

The flow over delta wings is dominated by two large counter-rotating leading-edge vortices that are formed by the roll up of vortex sheets shedding from leading edges. At a sufficiently high angle of attack, the vortices undergo a sudden expansion known as vortex breakdown [6,7], which has adverse aerodynamic effects on delta wing performance. Several investigations [8–13] demonstrated that thrust-vectoring jets at the trailing edge could delay vortex breakdown significantly, up to 50% of wing chord. Therefore, significant effects on the aerodynamic forces and moments on the wings are expected. The importance of the effects of the entrainment process and the interaction between the jet and wing vortices were reported [14,15]. Force measurements [13] revealed that the effect of nozzle geometry can be important because the entrainment effect of the jet depends on it. The jet–vortex interaction, distortion of jet vortices, and merging of wing and jet vortices are more pronounced for a rectangular nozzle and have a larger influence on the delta wing aerodynamics [13].

Previous studies mostly concentrated on the effect of trailing-edge jets on *slender* delta wings and vortex breakdown. *Nonslender* delta wings exhibit important differences with regard to the structure of vortical flows, vortex breakdown, and reattachment [16,17]. One of the distinct features of nonslender wings is the flow reattachment onto the wing surface. The effects of trailing-edge jets on nonslender delta wings are less known [13,18]. Although it appears that the delay of vortex breakdown becomes smaller with decreasing sweep angle [19], the effect of trailing-edge jets is substantial for the reattachment process. The maximum changes in the lift force occur near the stall angle [13] due to the earlier reattachment of the shear layer. Hence, near-stall and poststall performance of nonslender wings is expected to be significantly affected by thrust vectoring.

Previous studies have greatly improved our understanding of the effect of trailing-edge jets on delta wing aerodynamics. However, the

unsteady aspects remain to be fully investigated. For example, there is a lack of study on the effects of dynamic thrust vectoring, which is important for the flight control of UCAVs. Given that leading-edge vortices are highly unsteady [20], there is a need to better understand the unsteady aspects of the aerodynamics–propulsion interaction. For the dynamic thrust vectoring in which the jet pitch angle or the momentum flux varies as a function of time, significant time delays and hysteresis of the vortical flows and aerodynamic forces are expected. The response of wing vortical flow is expected to be similar, at least qualitatively, to that of unsteady wings. Hysteresis and time-lag of vortical flows and vortex breakdown over pitching or plunging wings are well known [21–25]. In this article, to simulate the dynamic thrust vectoring for a maneuver, the jet velocity (hence, momentum coefficient) was varied as a function of time using a control valve. One of the objectives of the present work is therefore to understand the effects of dynamically varying the momentum coefficient of the trailing-edge jet on delta wing aerodynamics, with an emphasis on quantifying hysteresis and phase lags. Both periodic and transient variations of the momentum coefficient $C\mu$ were investigated. Water-tunnel experiments were performed to simulate the unsteady thrust vectoring and quantify its effects by means of force measurements, flow visualization, and velocity measurements. Two delta wing models with sweep angles of 50 and 65 deg, representing nonslender and slender wings, respectively, were tested.

II. Methodology

A. Experimental Setup

Experiments were performed in a free-surface water tunnel (Eidetics Model 1520) with a $0.381 \times 0.508 \times 1.52$ m working section. The tunnel can provide freestream velocities in the range of $U_\infty = 0$–0.45 m/s, with a turbulence intensity of less than 1%, through a horizontal closed-loop continuous flow system. The tunnel has four viewing windows: three surrounding the test section and one downstream allowing axial viewing. The height of the test section above the floor allows flow visualization from below as well as from the sides. Two flat-plate delta wing models with sweep angles of $\Lambda = 50$ and 65 deg, representing nonslender and slender delta wings, respectively, were tested. The majority of the experiments were conducted for the nonslender delta wing, as the effect of dynamic thrust vectoring might be more important in this case. The models were constructed from an aluminum alloy. Both wings had a thickness of $t = 4.1$ mm and a chord length of $c = 100$ mm, giving a thickness-to-chord ratio of 4.1%. All models incorporated a sharp leading edge formed by bevelling the pressure surface by 45 deg; there was no bevelling at the trailing edge. Experiments were conducted at a freestream velocity of $U_\infty = 0.3$ m/s, giving Reynolds numbers ($Re = U_\infty c/\nu$, where U_∞ is the freestream velocity and ν is the fluid kinematic viscosity) $Re = 3.0 \times 10^4$ for both wings.

The dynamic thrust-vectoring jet system was fitted at the trailing edge (Fig. 1). Only one jet was used, simulating conditions as when a rolling moment is desired in flight. A convergent rectangular nozzle with a 2×12 mm exit cross section could be located at various spanwise locations. In this study, it was located at $y_{\text{jet}}/(b/2) = -0.6$ (approximately under the vortex core [13]) to achieve the maximum effect. The jet fluid was pumped in a pipe and then fed into the nozzle. During the experiments, there was no contact between the jet system and the wing, thus ensuring that any changes in the force measurements were solely from the blowing effects. The gap between the pipe feeding the nozzle and the wing was $0.02c$. This design allows easy change of the nozzle pitch angle β by rotating the pipe–nozzle assembly. The nozzle pitch angle β could also be varied dynamically to study the effect of jet pitch oscillations [26]. In this study, we kept the nozzle pitch angle at $\beta = 0$ deg, but varied the jet speed. A high-precision linear stepping motor valve was used to generate the dynamic variations of the jet speed. The stepping motor was controlled via a desktop PC using a Data Translation DT2112 data-acquisition card with 12 bit D/A conversion. The mean jet speed (or flow rate) was calibrated first, then the analog output from the card was taken to the stepping motor using feedback control to position the valve needle accurately.

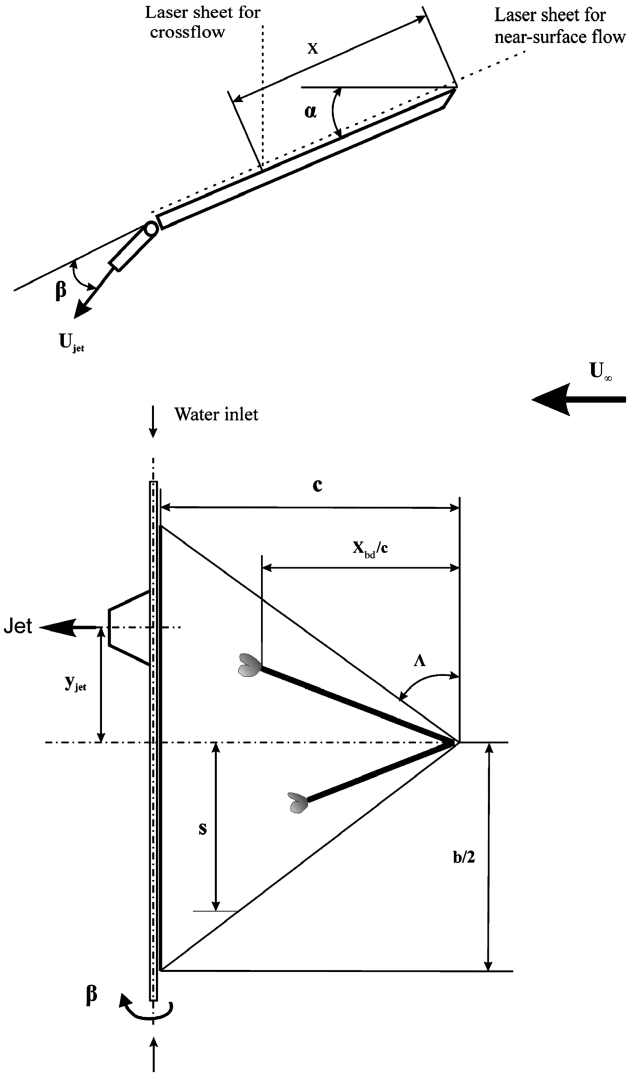

Fig. 1 Experimental arrangement.

For the purpose of comparison with previous data, experiments were carried out at the same range of jet momentum coefficient ($C\mu = \rho U_{\text{jet}}^2 A_{\text{jet}} / \frac{1}{2}\rho U_\infty^2 S_w$, where A_{jet} and S_w denote the cross-sectional area of the nozzle exit and surface area of the wing) from 0 to 0.43 for both wings. The values of the momentum coefficient used in the experiments are realistic for thrust-vectoring applications and also have been used by previous investigators [8–13]. Experiments were conducted for both periodic and transient (ramp) variations of the jet momentum coefficient. The periodic variation of the momentum coefficient $C\mu$ was constructed to follow a full cosine wave with a peak-to-peak amplitude of 0.43. For accelerating ($C\mu = 0 \rightarrow 0.43$) or decelerating ($C\mu = 0.43 \rightarrow 0$) transient variations, the momentum coefficient follows a half-cosine/sine wave from $t/T = 0$ to 0.5 and then remains constant (where T is the period of the corresponding full cosine wave). Three dimensionless frequencies, $f^* = 0.009$, 0.045, and 0.09 (where $f^* = fc/U_\infty$ and f is the oscillatory frequency of $C\mu$) were tested.

B. Force Measurements

Figure 2 presents the experimental arrangement for force measurements in the water tunnel. The wing models were mounted upside down with a streamlined support joined with an aluminum crossbar. The crossbar was screwed on a pair of load cells (Sensotec Model 31) attached on the assembly plate via fixed brackets, thus measuring the wing normal force. To reduce the preloading of the load cells, the

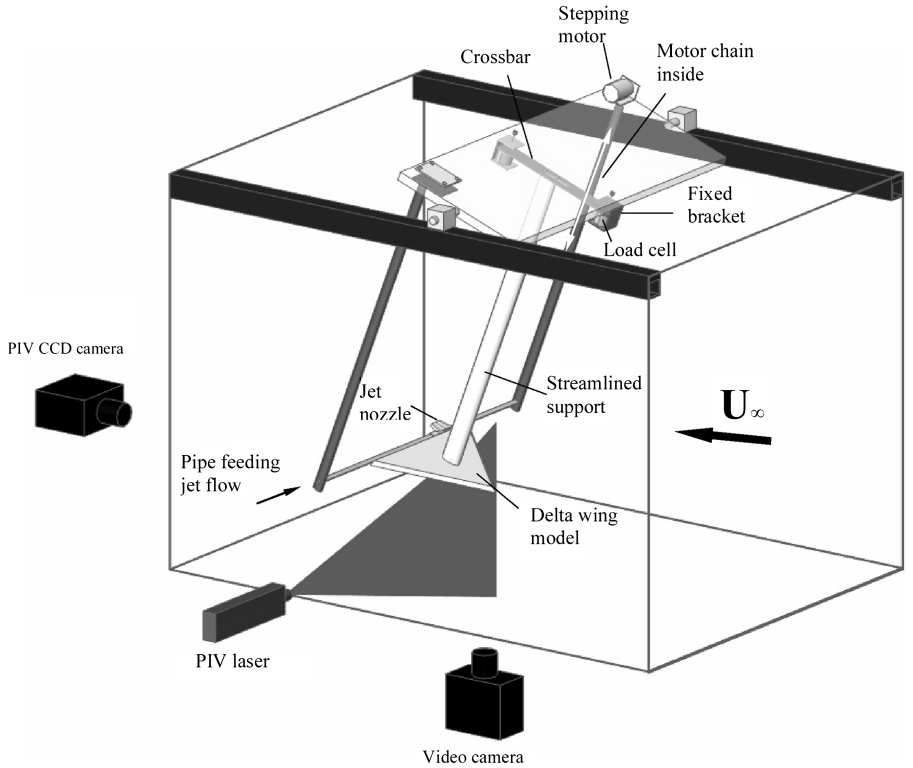

Fig. 2 Water-tunnel experimental setup.

wing models were constructed from acrylonitrile–butadiene–styrene copolymers. The angle of attack α was varied by swinging the whole experimental system, including the wing and jet system. Signals from the load cells were simultaneously digitized and amplified

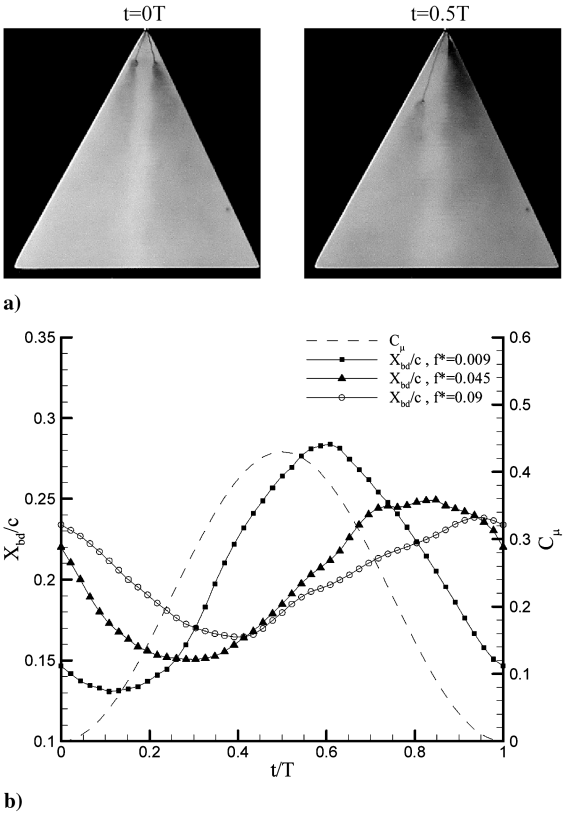

Fig. 3 Effect of periodic trailing-edge blowing on vortex breakdown location: a) Food-coloring dye flow visualization over slender delta wing ($\Lambda = 65$ deg) with periodic trailing-edge blowing, $f^* = 0.009$; b) phase-averaged vortex breakdown location as a function of normalized time t/T, $\alpha = 35$ deg.

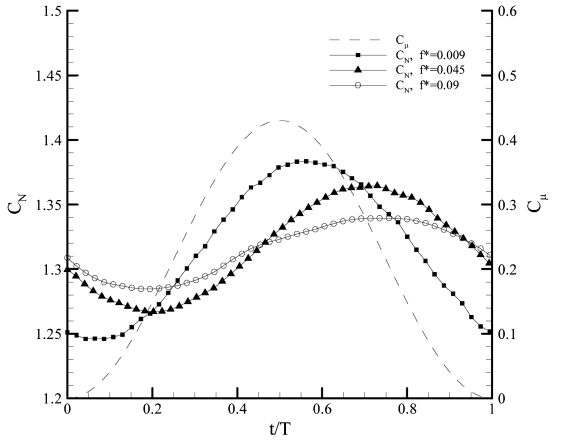

Fig. 4 Variation of phase-averaged normal force coefficient of nonslender delta wing with periodic trailing-edge blowing as a function of time t/T, $\Lambda = 50$ deg, $\alpha = 25$ deg.

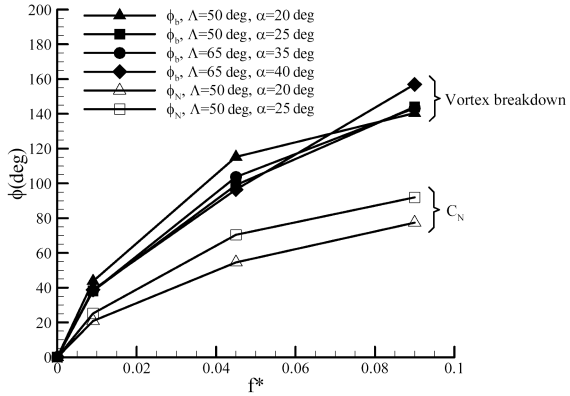

Fig. 5 Variation of phase lags of the dynamic response of normal force (ϕ_N) and vortex breakdown (ϕ_b) as a function of dimensionless blowing frequency.

using a 12 bit A/D board and a personal computer at a sampling frequency of 100 Hz per channel. The duration of each record was 30 s or 30 cycles of the periodically varying $C\mu$, whichever was longer. This record length was found to be sufficiently long for the phase-averaged force measurements. The measured normal force was then normalized by qS_w, where $q = \frac{1}{2}\rho U_\infty^2$ is the freestream dynamic pressure. The experimental uncertainty of the normal force coefficient was estimated to be 1%. The estimates of the uncertainty of the measurements were arrived at based on the standard uncertainty calculations (such as the Kline–McClintock method) and given in Jiang's Ph.D. thesis [26]. For the validation of the force balance, measurements of the normal force coefficient were compared with previous data and excellent agreement was found [26].

Force measurements were carried out for the nonslender delta wing only. Because previous studies suggested that the maximum effect of trailing-edge jets occurs near the wing stall angle [13], force measurements were therefore carried out at angles of attack of $\alpha = 20$ and 25 deg, representing stall and poststall incidences, respectively, for the nonslender wing ($\Lambda = 50$ deg).

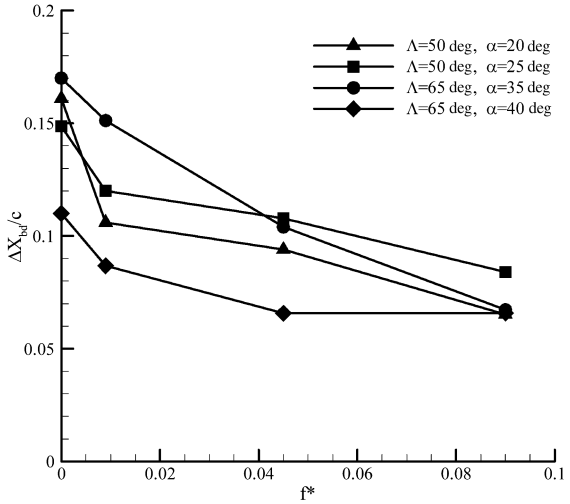

Fig. 6 Variation of peak-to-peak amplitude of vortex breakdown location X_{bd} as a function of dimensionless frequency of periodic trailing-edge blowing.

C. Flow Visualization

Flow visualization of the leading-edge vortices and vortex breakdown was conducted. To visualize the leading-edge vortex trajectories, food-coloring dye, diluted 1:4 with water, was released at the wing apex. A digital video camera recorder was used to record the leading-edge vortex trajectories at a rate of 25 frames per second and a resolution of 570,000 pixels. The captured images were interfaced to a desktop computer via the commercial software package Pinnacle Studio DV, enabling real-time viewing of the wing flow visualization and the capture of camera images and video recordings. The captured images were magnified and analyzed with a MATLAB® code. The vortex breakdown locations were then identified. The experimental uncertainty in locating the vortex breakdown position was estimated to be approximately 1%c. The time histories of the vortex breakdown location were obtained by analyzing the video recording of flow visualization frame by frame. Experiments were conducted at $\alpha = 20$ and 25 deg for the nonslender wing and at $\alpha = 35$ and 40 deg for the slender wing. Other experimental conditions were the same as for the force measurements.

D. Particle Image Velocimetry Measurements

To obtain quantitative information on the flowfield, particle image velocimetry (PIV) measurements were carried out in the water tunnel. The experimental conditions were the same as those for flow visualization tests. The model surface was painted black to minimize reflection. The flow was seeded with commercially available hollow glass particles with mean diameter of 4 μm. The PIV camera was placed near the downstream viewing window to measure the velocity field in a crossflow plane (see Fig. 2). In additional experiments, the camera was placed underneath the tunnel working section and the light sheet was placed parallel and close to the wing surface (1 mm) to reveal the near-surface flow pattern (as sketched in Fig. 1). Illumination was provided by the laser sheets generated by a combination of cylindrical and spherical lenses from a pair of pulsed mini Nd:YAG lasers with a maximum energy of 120 mJ per pulse. The digital particle images were taken using an 8-bit CCD camera with a resolution of 4.2×10^6 pixels. The commercial software package Insight v6.0 and a Hart cross-correlation algorithm were

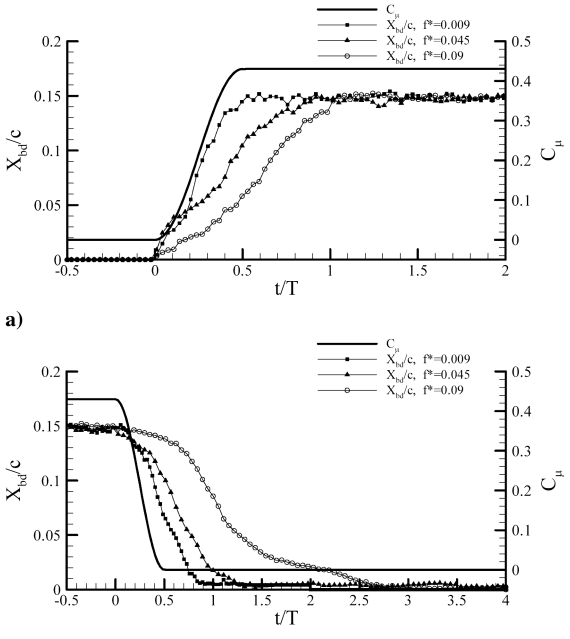

Fig. 7 Dynamic response of vortex breakdown over nonslender delta wing with transient trailing-edge blowing, $\Lambda = 50$ deg, $\alpha = 25$ deg: a) accelerating $C\mu$, and b) decelerating $C\mu$.

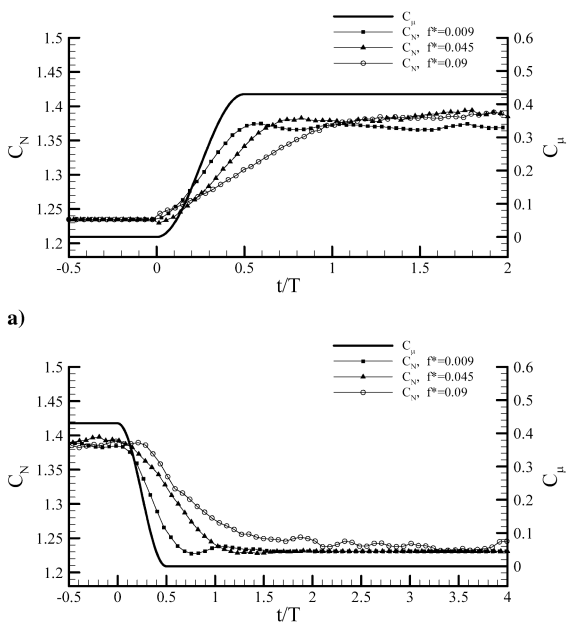

Fig. 8 Dynamic response of normal force coefficient over nonslender delta wing with transient trailing-edge blowing, $\Lambda = 50$ deg, $\alpha = 25$ deg: a) accelerating $C\mu$, and b) decelerating $C\mu$.

used to analyze the images. In image processing, an interrogation window size of 32×32 pixels was used, thus producing velocity vectors for further processing. The effective grid size was varied from 1.8 mm in crossflow planes to 3.0 mm in a plane near the wing surface. The estimated uncertainty for velocity measurements is 2% of the freestream velocity U_∞. The pulsing laser sheet and PIV camera were triggered by analog pulses generated from the Data Translation DT2112 data-acquisition card, which was used to control the stepping motor valve, thus enabling phase-locked PIV measurements. For each case, sequences of 100 instantaneous frames were taken and phase-averaged velocity and vorticity fields were calculated.

III. Results

As discussed earlier, the effect of trailing-edge jets is thought to be more important for nonslender wings, in particular near the stall and in the poststall regimes. Hence, the majority of the experiments with unsteady blowing were conducted for the nonslender delta wing, although some comparison with the slender wing is also presented.

A. Periodic Trailing-Edge Blowing

The jet momentum coefficient $C\mu$ of periodic trailing-edge blowing follows a cosine wave, $C\mu = 0.215 + 0.215\cos(2\pi f t + \pi)$, with a peak-to-peak amplitude of 0.43 and a time-averaged value of 0.215, where f is the oscillatory frequency of $C\mu$. Figure 3a presents the typical flow visualization images of leading-edge vortices over slender delta wing ($\Lambda = 65$ deg) at an incidence of $\alpha = 35$ deg and a frequency of $f^* = 0.009$. Initially, at $t/T = 0$ and $C\mu = 0$, the breakdown of the leading-edge vortices appears symmetric and occurs at $x/c \approx 0.15$. At $t/T = 0.5$ and $C\mu = 0.43$, it can be observed that the vortex breakdown of the jet (left) side was delayed to $x/c \approx 0.3$, whereas the vortex breakdown at the right-hand side occurs closer to the wing apex. The present observation is consistent with the steady trailing-edge blowing for the same configuration [13].

The phase-averaged variations of vortex breakdown location X_{bd}/c over the slender wing ($\Lambda = 65$ deg) at the same angle of attack are presented in Fig. 3b. For each f^* tested, the response of X_{bd}/c to the periodically varying $C\mu$ exhibits a periodic variation with a phase lag. The phase lag tends to increase with increasing f^*, whereas the amplitude of X_{bd}/c tends to be decreasing with increasing f^*. Similar trends of X_{bd}/c were also obtained for the nonslender wing ($\Lambda = 50$ deg) (not shown here). Figure 4 presents the variation of the phased-averaged normal force coefficient C_N for the nonslender wing ($\Lambda = 50$ deg) at $\alpha = 25$ deg. Similar to the variations of the breakdown location X_{bd}/c, the normal force coefficient C_N also follows a periodic cosine wave, with increasing phase lag and decreasing amplitude as f^* is increased.

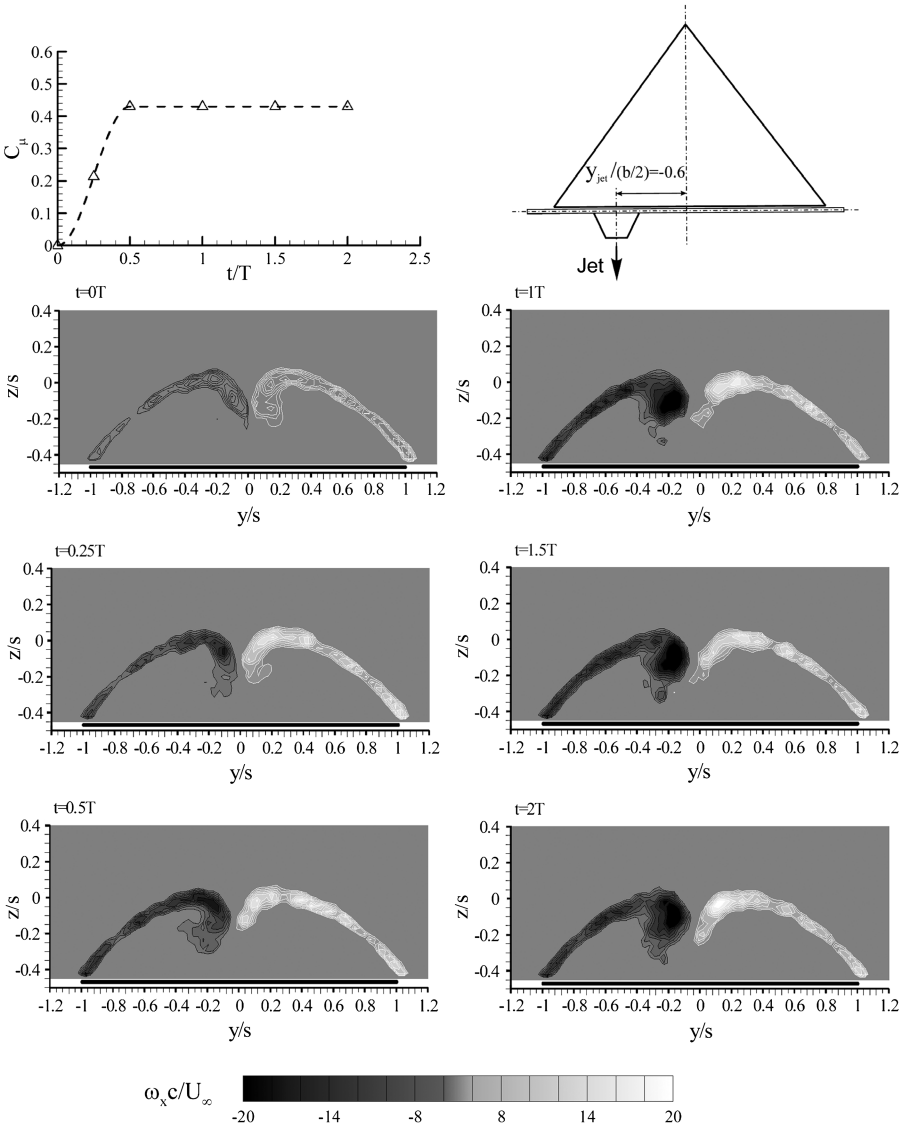

Fig. 9 Phase-averaged vorticity in a crossflow plane over nonslender delta wing for accelerating momentum coefficient, $\alpha = 25$ deg, $x/c = 0.3$, $f^* = 0.09$. The inset shows the variation of the momentum coefficient with symbols showing the instants of PIV measurements.

The dependence of the phase lag ϕ of X_{bd}/c and C_N on the dimensionless blowing frequency f^* is presented in Fig. 5 for both wings. The phase lags were calculated from the Fourier series analysis of the phase-averaged variation of the quantities. It can be observed that X_{bd}/c and C_N exhibit similar trends of increasing ϕ with increasing f^*. This is similar to the findings of previous investigations for unsteady wings [21–25]. The phase lag ϕ_b of X_{bd}/c for the slender delta wing is comparable to those of the nonslender delta wing. However, the phase lag ϕ_N of C_N is smaller than the phase lag ϕ_b of X_{bd}/c. This observation suggests that the development of vortex breakdown lags behind wing aerodynamic forces. Polhamus's theory [27] predicts that the vortex lift is only a part of the total lift over delta wings. The present observation suggests that potential lift also contributes to the dynamic response of wing aerodynamics.

Figure 6 presents the dependence of the peak-to-peak amplitude of the phase-averaged breakdown location X_{bd}/c on the dimensionless frequency f^*. For both $\Lambda = 65$ deg and $\Lambda = 50$ deg wings, with continuous trailing-edge blowing ($f^* = 0$), X_{bd}/c exhibits the largest amplitudes. When the periodic trailing-edge blowing is applied, the peak-to-peak amplitude of the vortex breakdown location $\Delta X_{bd}/c$ tends to decrease. This amplitude attenuation is similar for both the slender and nonslender wings. This observation is also similar to the findings of previous investigations for unsteady wings [21–25].

If it is assumed that the response of X_{bd} and C_N to periodic trailing-edge blowing is similar to that of a first-order system to a sinusoidal input [24,25], the time constant τ of the dynamic response can be estimated from the measured phase lags. The estimated $\tau U_\infty/c$ for the breakdown location X_{bd} varied in the range of 4.3–5.6 for both wings, which is somewhat larger than those reported in the literature for the oscillating wings ($\tau U_\infty/c = 1$–2) [24,25,28]. Also, the time constant for oscillating nozzles was in the range of 0.5–1.5 for both wings [26]. Hence, the time constant appears to be larger for the dynamic jet than for the oscillating wings and nozzles. For the nonslender wing ($\Lambda = 50$ deg), the normalized time constant $\tau U_\infty/c$ is estimated from C_N in the range of 1.7–3.3, smaller than $\tau U_\infty/c$ of X_{bd}, suggesting that a significant role is played by the potential lift contribution.

B. Transient Trailing-Edge Blowing

Figure 7 presents the dynamic response of X_{bd}/c to an accelerating jet momentum coefficient (Fig. 7a) and also to a decelerating jet momentum coefficient (Fig. 7b) for the nonslender delta wing at a poststall incidence of $\alpha = 25$ deg. The time histories of $C\mu$ are also included in Fig. 7. The transient $C\mu$ followed the half-cosine/sine wave, that is, from $t = 0$ to 0.5 T, with the same corresponding dimensionless frequencies f^* as periodic blowing configurations (Sec. III.A), (i.e., $f^* = 0.009$, 0.045 and 0.09). For this poststall incidence, the steady-state locations of vortex breakdown are $X_{bd}/c = 0$ at $C\mu = 0$ and 0.15 at $C\mu = 0.43$. Figure 7a indicates that, as $C\mu$ was increased from 0 to 0.43 as a half-sine wave, X_{bd}/c gradually increased to its steady value with a time delay. This is similar to the response of vortex breakdown for transient pitch-up

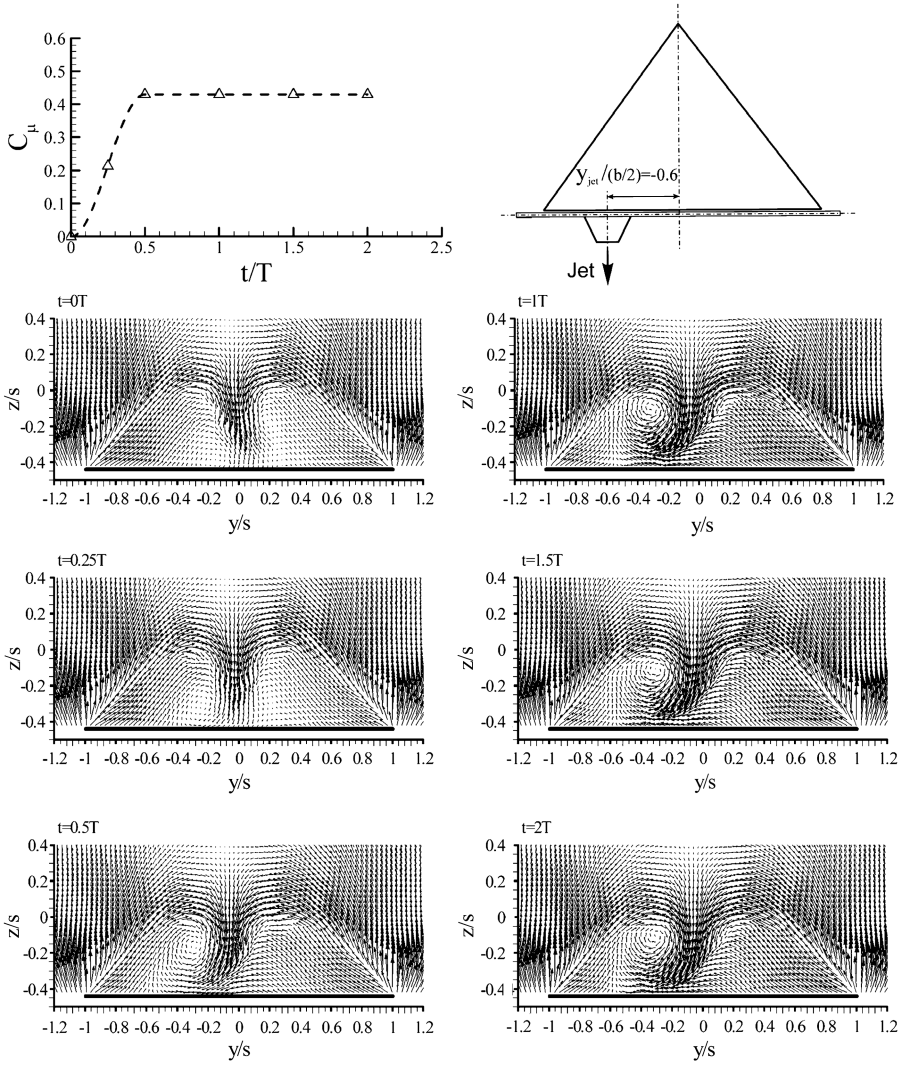

Fig. 10 Phase-averaged velocity vectors in a crossflow plane over nonslender delta wing for accelerating momentum coefficient, $\alpha = 25$ deg, $x/c = 0.3$, $f^* = 0.09$. The inset shows the variation of the momentum coefficient with symbols showing the instants of PIV measurements.

and pitch-down motions of delta wings [29]. It is seen in Fig. 7a that the time delay (normalized with the period) increases with increasing frequency. The results reveal the differences in the responses of vortex breakdown and vortex reformation.

Similar trends were also found for the decelerating blowing cases (Fig. 7b). However, the time delays are significantly larger than those of the accelerating case (note that the scales of the horizontal axis are different in parts a and b). Hence, characteristic response times for accelerating and decelerating jets appear to be different. It is interesting that this behavior is similar to the different flow structures reported at the same angle of attack during the pitch-up and pitch-down motions of a delta wing [30]. Also, different time constants for the upstream and downstream motion of the breakdowns were reported in response to an oscillating fin over a delta wing [31]. The normal force coefficient C_N exhibits similar trends to X_{bd}/c (see Fig. 8). Similar to X_{bd}/c (Fig. 7), C_N gradually increased to its steady value with a time delay for the accelerating jet. For the decelerating jet, the time delays were larger than those of the accelerating case.

PIV measurements were conducted to further investigate the effects of transient trailing-edge blowing on vortical flow characteristics over the nonslender delta wing. Figure 9 presents the phase-averaged vorticity field in a crossflow plane at $x/c = 0.3$ and $\alpha = 25$ deg with an accelerating momentum coefficient for $f^* = 0.09$. Initially ($t = 0$, $C\mu = 0$), the flow pattern was symmetric and the separated shear layers touched each other near the wing centerline. In this stalled flow, the shear layers were symmetrically placed and had low vorticity values. The corresponding velocity vectors in the crossflow plane (see Fig. 10) confirmed that there is no reattachment outboard of the wing centerline. At $t = 0.25T$, the vorticity on the jet (left) side became stronger and the shear layer started moving outboard (see Fig. 9), due to the jet entrainment effect. When $C\mu$ reached the maximum value of 0.43 at $t = 0.5T$, the shear layer on the jet side started to form a vortical structure (Fig. 9) and the high-velocity region came closer to the wing surface (Fig. 10). For $t = T$ and larger times, the phase-averaged flow patterns did not change much. The maximum value of the magnitude of the normalized vorticity $\omega_x c/U_\infty$ was larger on the jet side, and the corresponding vortical flow was more axisymmetric.

Similarly, the crossflow PIV measurements for the decelerating trailing-edge blowing are shown in Figs. 11 and 12. Initially ($t = 0$, $C\mu = 0.43$), the more axisymmetric vortical structure is seen on the jet side, with larger values of vorticity. As $C\mu$ decreased to 0 at $t = 0.5T$, the flow pattern remained similar to that at $t = 0$, but with a slightly reduced magnitude of $\omega_x c/U_\infty$. At $t = T$ and later, the magnitude of $\omega_x c/U_\infty$ on the jet side was reduced considerably, and the strong leading-edge vortical structure disappeared, suggesting that the flow eventually stalls. The corresponding velocity vectors in Fig. 12 confirm the same observations, and also reveal the inboard movement of the vortex. Further quantitative information, such as the circulation, was also obtained from these measurements, as discussed in the next paragraph.

Figure 13 presents the variations of circulation $\Gamma/U_\infty c$ as a function of t/T for $f^* = 0.09$. The circulation was calculated as the line integral of velocity around a rectangle that encloses the vortex on

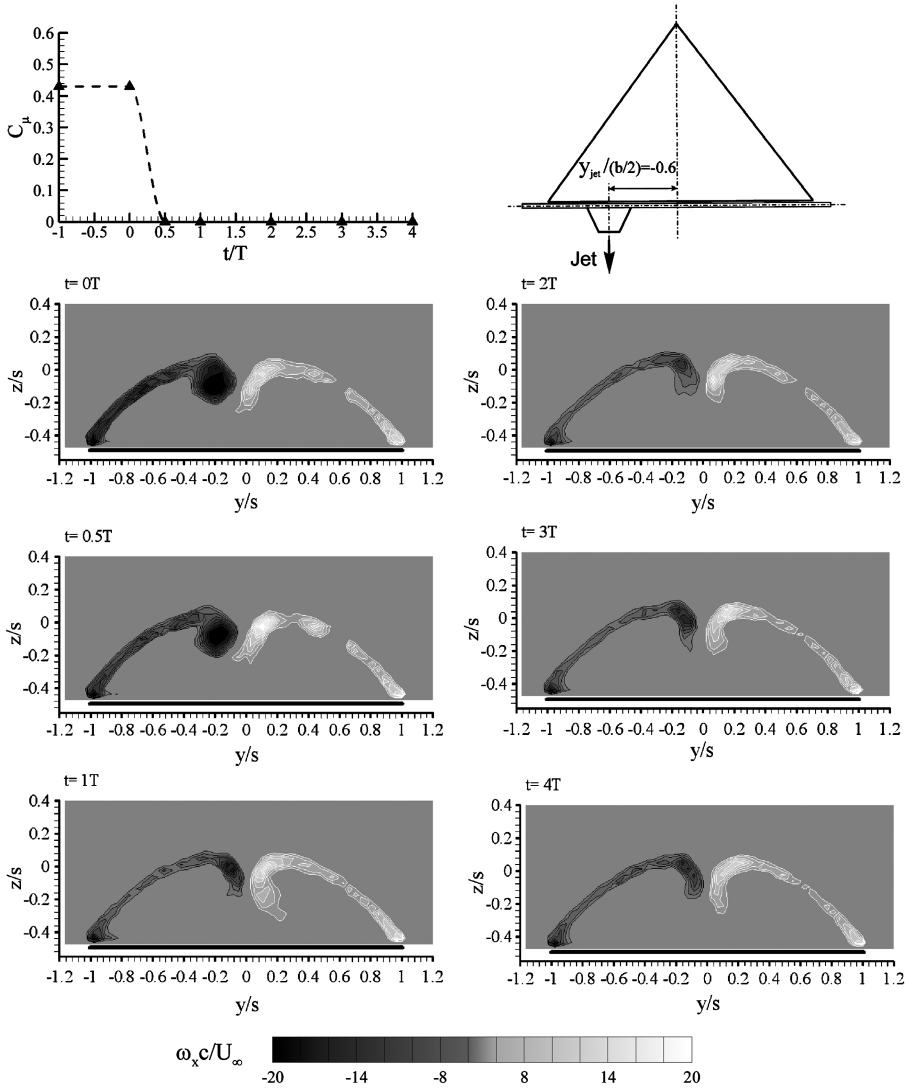

Fig. 11 Phase-averaged vorticity in a crossflow plane over nonslender delta wing for decelerating momentum coefficient, $\alpha = 25$ deg, $x/c = 0.3$, $f^* = 0.09$. The inset shows the variation of the momentum coefficient with symbols showing the instants of PIV measurements.

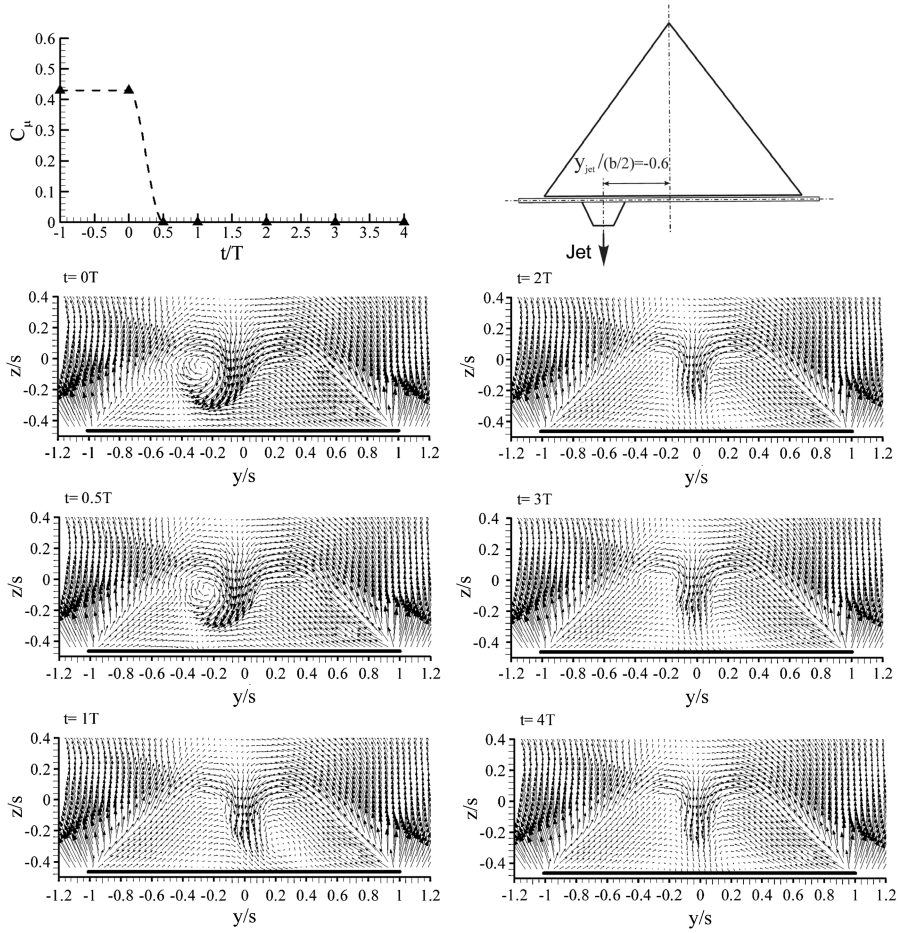

Fig. 12 Phase-averaged velocity vectors in a crossflow plane over nonslender delta wing for decelerating momentum coefficient, $\alpha = 25$ deg, $x/c = 0.3$, $f^* = 0.09$. The inset shows the variation of the momentum coefficient with symbols showing the instants of PIV measurements.

the jet (left) side. It can be observed that the trends of $\Gamma/U_\infty c$ resemble those of C_N (Fig. 8). For the accelerating jet, the normalized circulation $\Gamma/U_\infty c$ reached the steady-state value around $t/T = 1.5$. However, the normalized circulation does not appear to reach the steady-state value even at $t/T = 4$ for the decelerating jet. The effects of acceleration and deceleration of the jet momentum coefficient are all similar for the variations of breakdown location (Fig. 7), normal force coefficient (Fig. 8), and circulation (Fig. 13).

The time constant was estimated from these data by assuming that the response is similar to that of a first-order system to a step function input [24,25]. The time required for the variable to reach 95% of the steady-state value was estimated as 3τ, where τ is the time constant of the first-order system. Figure 14 presents the normalized time constant τ/T obtained from X_{bd}, C_N, and $\Gamma/U_\infty c$ as a function of f^*. It is seen that, for both accelerating and decelerating jet blowing cases, the time constant normalized by the period τ/T increases with f^*, and the time constant is several times larger for the decelerating jet case. The time constant of C_N is smaller than that of X_{bd}/c, suggesting that vortex lift as well as potential lift contributions are important. The time constant of circulation is close to that of breakdown.

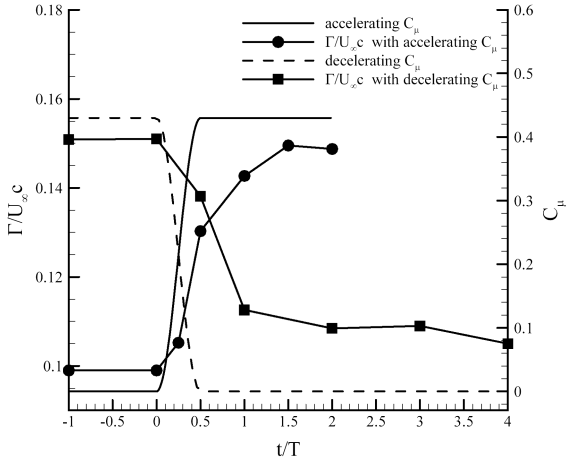

Fig. 13 Variation of normalized circulation of vortical flow in a crossflow plane at $x/c = 0.3$ over nonslender delta wing with transient trailing-edge blowing, $f^* = 0.09$, $\alpha = 25$ deg, $\Lambda = 50$ deg.

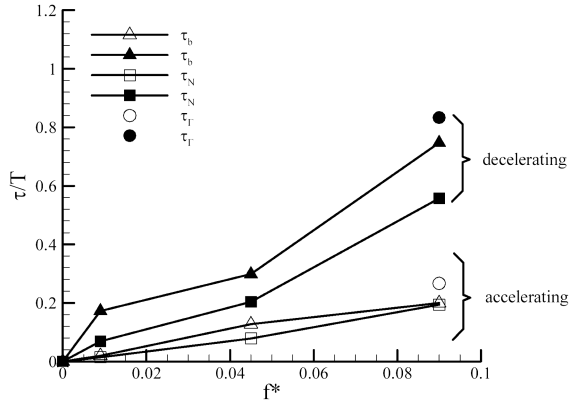

Fig. 14 Variation of normalized time constants τ/T of vortex breakdown, normal force coefficient, and circulation over nonslender delta wing with transient trailing-edge blowing, $\alpha = 25$ deg, $\Lambda = 50$ deg.

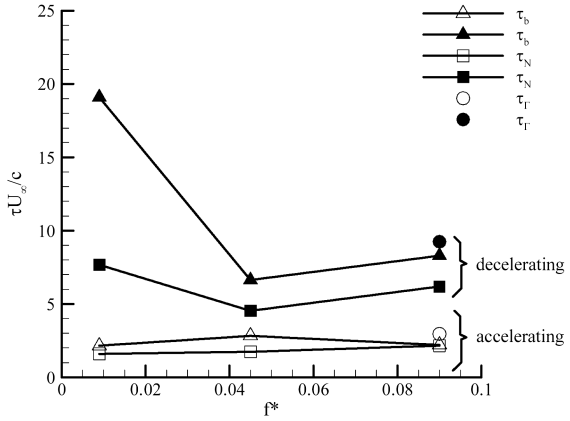

Fig. 15 Variation of normalized time constant $\tau U_\infty/c$ of vortex breakdown, normal force coefficient and circulation over nonslender delta wing with transient trailing-edge blowing, $\alpha = 25$ deg, $\Lambda = 50$ deg.

The corresponding variation of the time constant normalized by the convective time unit, $\tau U_\infty/c$, is presented in Fig. 15. Note that the estimates for the highest frequency parameter are the most reliable because of the assumption of the step function input in the calculations. The estimated $\tau U_\infty/c$ for the decelerating case varied in the range of 6–9, whereas it is around 2–3 for the accelerating case.

These results were obtained for the poststall angle of attack of $\alpha = 25$ deg. The effects of transient trailing-edge blowing on wing flow characteristics were also studied for an angle of attack near the stall, $\alpha = 20$ deg. Figures 16 and 17 show the phase-averaged streamline patterns near the wing surface at $\alpha = 20$ deg. For the accelerating jet case of $f^* = 0.09$, at $t = 0$ ($C\mu = 0$), the flow pattern is fairly symmetric about the wing centerline with closed spiraling streamline patterns (nodes) on both sides near the wing apex (Fig. 16). Note that the leading-edge vortex breakdown occurred near the wing apex at $\alpha = 20$ deg, which is the stall angle of the $\Lambda = 50$ deg wing [13]. As $C\mu$ increased to 0.43 at $t = 0.5T$, the reattachment on the jet (left) side occurs slightly before the centerline and the closed spiraling streamline pattern near the wing apex

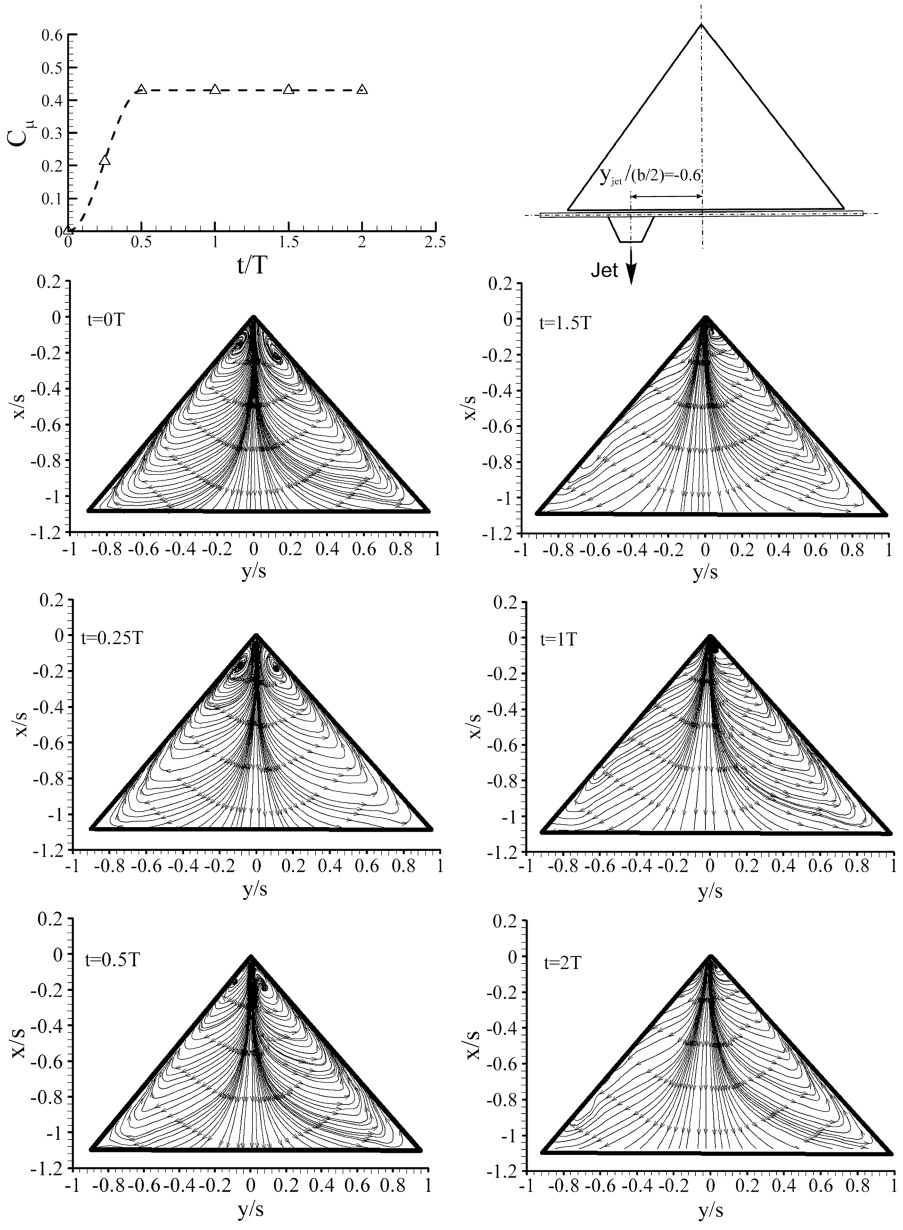

Fig. 16 Near-surface streamline pattern for the nonslender ($\Lambda = 50$ deg) wing with accelerating trailing-edge blowing, $\alpha = 20$ deg, $f^* = 0.09$. The inset shows the variation of the momentum coefficient with symbols showing the instants of PIV measurements.

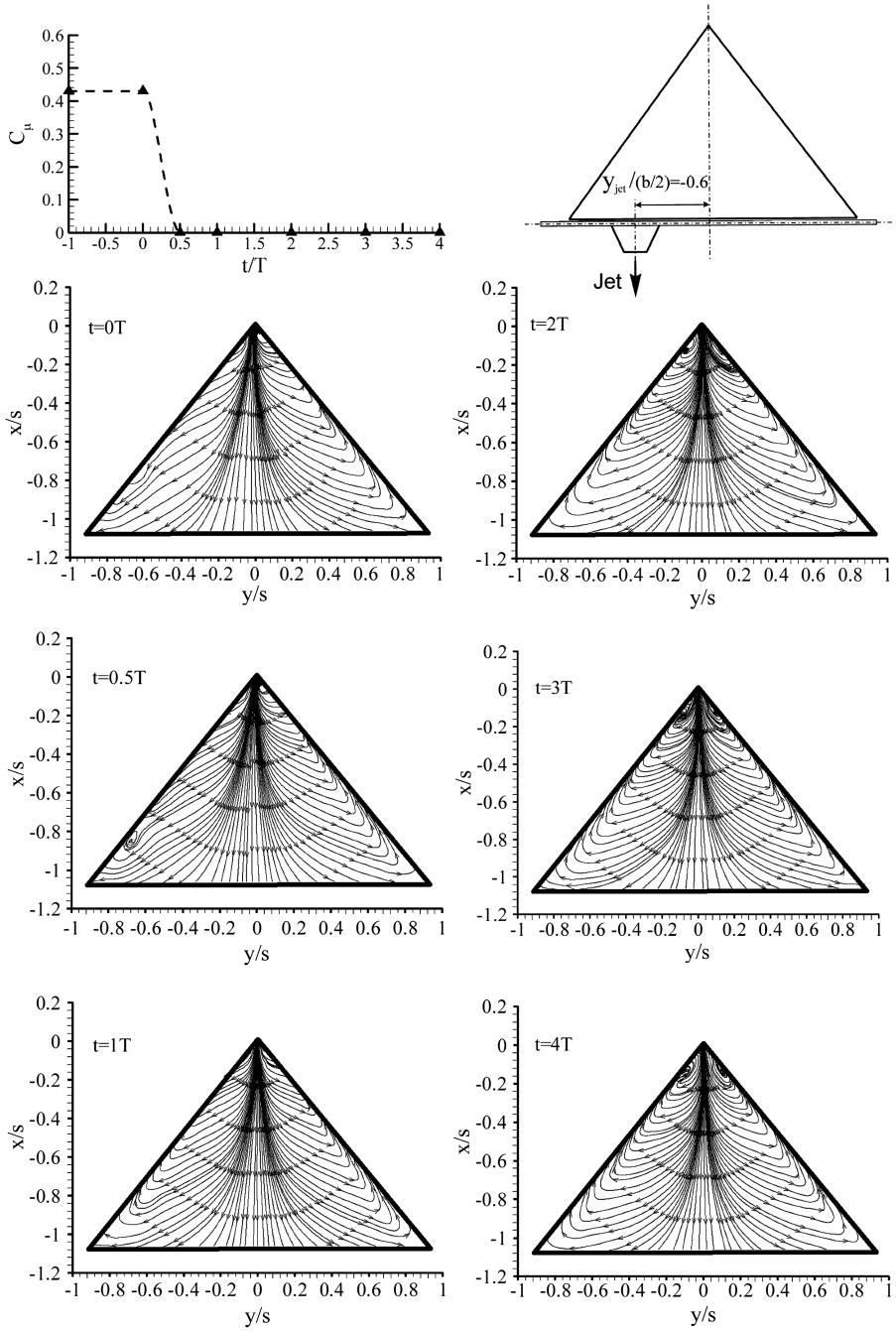

Fig. 17 Near-surface streamline pattern for the nonslender ($\Lambda = 50$ deg) wing with decelerating trailing-edge blowing, $\alpha = 20$ deg, $f^* = 0.09$. The inset shows the variation of the momentum coefficient with symbols showing the instants of PIV measurements.

persists only at the right side with a much smaller scale than that at $t = 0$. After $t = T$, two separate reattachments occur on the wing surface, and the reattachment on the jet side is more outboard. As a result, the flowfield appears asymmetric about the wing centerline. It is seen in Fig. 16 that the flow pattern for $C\mu = 0$ exhibits a single reattachment near the wing symmetry plane, whereas two separate reattachment lines can be identified for jet blowing.

The case of decelerating trailing-edge blowing is shown in Fig. 17. At $t = 0$ ($C\mu = 0.43$), the flow pattern appears similar to that of steady trailing-edge blowing [13], that is, two separate asymmetric reattachment lines. As the jet momentum decreases for $t = 0.5T$ and T, the reattachment lines move toward the wing centerline and the flow becomes more symmetric. After $t = 2T$, the flow becomes fairly symmetric and the closed spiraling streamline patterns recovers on both sides near the wing apex. The estimated time constant $\tau U_\infty c$ for the wing stall angle of $\alpha = 20$ deg is shown in Fig. 18, which exhibits similar trends to that of $\alpha = 25$ deg. The range of time constants for accelerating and decelerating jets is also similar to that of the poststall angle of attack.

C. Effects of Wing Sweep Angle

To study the effect of sweep angle on the dynamic response characteristics of wing flow to transient trailing-edge blowing, flow visualization and PIV measurements over the slender ($\Lambda = 65$ deg) delta wing were carried out at stall ($\alpha = 35$ deg) and poststall ($\alpha = 40$ deg) incidences. The variations of breakdown location X_{bd}/c and circulation $\Gamma/U_\infty c$ with time (not shown here) are qualitatively similar to the nonslender delta wing case. Figure 19 summarizes the time constant $\tau U_\infty/c$ of X_{bd} and $\Gamma/U_\infty c$. It can be observed that, similar to nonslender wing, $\tau U_\infty/c$ of accelerating blowing configurations are smaller than $\tau U_\infty/c$ of decelerating blowing configurations. Furthermore, the magnitudes of $\tau U_\infty/c$ are comparable with those of nonslender ($\Lambda = 50$ deg) wing cases.

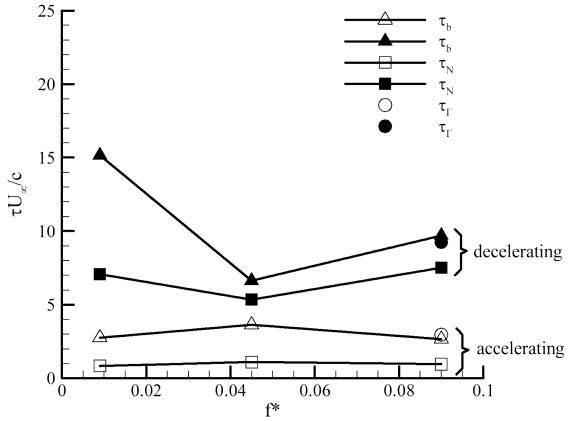

Fig. 18 Variation of normalized time constant $\tau U_\infty/c$ of vortex breakdown, normal force coefficient and circulation over nonslender delta wing with transient trailing-edge blowing, $\alpha = 20$ deg, $\Lambda = 50$ deg.

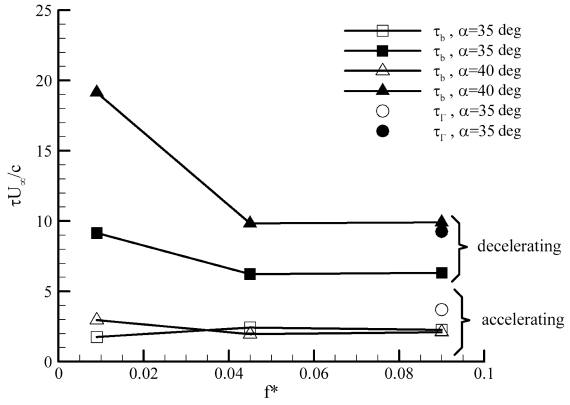

Fig. 19 Variation of normalized time constant $\tau U_\infty/c$ of vortex breakdown and circulation over slender delta wing with transient trailing-edge blowing, $\Lambda = 65$ deg, $\alpha = 35$ and 40 deg.

IV. Conclusions

Flow visualization, particle image velocimetry and force measurements were conducted to investigate the effects of unsteady trailing-edge thrust vectoring on delta wing aerodynamics. Periodic and transient variations of the jet momentum coefficient were considered. Experiments were carried out on both slender ($\Lambda = 65$ deg) and nonslender ($\Lambda = 50$ deg) stationary delta wings at stall and poststall incidences. The following conclusions can be drawn:

1) For the periodic trailing-edge blowing, the dynamic response of the leading-edge vortex breakdown location X_{bd} and normal force coefficient C_N exhibit similar periodic trends with phase lags. The phase lag ϕ increases with increasing frequency f^* of the periodic variations of the momentum coefficient. For the variation of vortex breakdown, the estimated time constant is larger than those reported in the literature for unsteady wings undergoing pitching or plunging, and for oscillating nozzles. The phase lag of the normal force is smaller than that of the vortex breakdown, indicating that both the potential lift and vortex lift play a role in the dynamic response.

2) For the transient trailing-edge blowing, both the breakdown location and normal force reached their steady-state values with a time delay for the nonslender delta wing at a poststall incidence. This is similar to the response of vortex breakdown for transient pitch-up or pitch-down motions of delta wings. The time delay for the decelerating jet is significantly larger than that for the accelerating jet. Phase-averaged PIV measurements confirmed that the leading-edge vortex was gradually reformed from the stalled flow under the effect of transient accelerating blowing, or vice versa for decelerating transient blowing. Variation of the calculated circulation and estimated time constant reveal similar results to those of vortex breakdown and normal force. The normalized time constant $\tau U_\infty/c$ for the decelerating case varied in the range of 6–9, whereas it is around 2–3 for the accelerating case.

3) Similar results were obtained at the stall angle of attack. Near-surface streamline patterns revealed how the reattachment of the shear layers varied in response to transient blowing. The range of time constants for accelerating and decelerating jets is also similar to that of the poststall angle of attack.

4) The effects of transient trailing-edge blowing on the slender ($\Lambda = 65$ deg) delta wing are similar to those of the nonslender ($\Lambda = 50$ deg) wing. Flow visualization and PIV measurements indicate similar magnitudes of $\tau U_\infty/c$ to the nonslender wing case.

Acknowledgments

This work is jointly funded by the Engineering and Physical Sciences Research Council and the Ministry of Defence in the United Kingdom, as well as by the Research Councils United Kingdom Academic Fellowship in Unmanned Air Vehicles.

References

[1] Earnshaw, P. B., and Lawford, J. A., "Low-Speed Wind-Tunnel Experiments on a Series of Sharp-Edged Delta Wings," Aeronautical Research Council R&M 3424, 1964.

[2] Wentz, W. H., Jr., and Kohlman, D. L., "Vortex Breakdown on Slender Sharp-Edged Wings," *Journal of Aircraft*, Vol. 8, No. 3, 1971, pp. 156–161.
doi:10.2514/3.44247

[3] Lee, M., and Ho, C. M., "Lift Force of Delta Wings," *Applied Mechanics Reviews*, Vol. 43, No. 9, 1990, pp. 209–221.

[4] Gursul, I., "Recent Developments in Delta Wing Aerodynamics," *The Aeronautical Journal*, Sept. 2004, pp. 437–452.

[5] Gursul, I., "Vortex Flows on UAVs: Issues and Challenges," *The Aeronautical Journal*, Dec. 2004, pp. 597–610.

[6] Werle, H., "Quelques Resultants Experimentaux sur les Ailes en Fleche, aux Faibles Vitesses, Obtenus en Tunnel Hydrodynamique," *Recherche Aéronautique*, Vol. 41, Sept.–Oct. 1954, pp. 15–21.

[7] Lambourne, N. C., and Bryer, D. W., "The Bursting of Leading Edge Vortices: Some Observation and Discussion of the Phenomenon," Aeronautical Research Council, R&M 3282, 1962.

[8] Helin, H. E., and Watry, C. W., "Effects of Trailing-Edge Jet Entrainment on Delta Wing Vortices," *AIAA Journal*, Vol. 32, No. 4, 1994, pp. 802–804.
doi:10.2514/3.12056

[9] Shih, C., and Ding, Z., "Trailing-Edge Jet Control of Leading-Edge Vortices of a Delta Wing," *AIAA Journal*, Vol. 34, No. 7, 1996, pp. 1447–1457.
doi:10.2514/3.13252

[10] Vorobieff, P. V., and Rockwell, D. O., "Vortex Breakdown on Pitching Delta Wing: Control by Intermittent Trailing-Edge Blowing," *AIAA Journal*, Vol. 36, No. 4, 1998, pp. 585–589.
doi:10.2514/2.409

[11] Mitchell, A. M., Barberis, D., Molton, P., and Delery, J., "Control of Leading-Edge Vortex Breakdown by Trailing Edge Injection," *Journal of Aircraft*, Vol. 39, No. 2, 2002, pp. 221–226.
doi:10.2514/2.2942

[12] Phillips, S., Lambert, C., and Gursul, I., "Effect of a Trailing-Edge Jet on Fin Buffeting," *Journal of Aircraft*, Vol. 40, No. 3, 2003, pp. 590–599.
doi:10.2514/2.3135

[13] Wang, Z.-J., Jiang, P., and Gursul, I., "Effect of Thrust Vectoring Jets on Delta Wing Aerodynamics," *Journal of Aircraft*, Vol. 44, No. 6, 2007, pp. 1877–1888.
doi:10.2514/1.30568

[14] Wang, F. Y., Proot, M. M. J., Charbonnier, J. M., and Sforza, P. M., "Near-Field Interaction of a Jet with Leading-Edge Vortices," *Journal of Aircraft*, Vol. 37, No. 5, 2000, pp. 779–785.
doi:10.2514/2.2700

[15] Wang, F. Y., and Zaman, K. B. M. Q., "Aerodynamics of a Jet in the Vortex Wake of a Wing," *AIAA Journal*, Vol. 40, No. 3, 2002, pp. 401–407.
doi:10.2514/2.1669

[16] Taylor, G., and Gursul, I., "Buffeting Flows over a Low-Sweep Delta Wing," *AIAA Journal*, Vol. 42, No. 9, Sept. 2004, pp. 1737–1745.
doi:10.2514/1.5391

[17] Gursul, I., Gordnier, R., and Visbal, M., "Unsteady Aerodynamics of Nonslender Delta Wings," *Progress in Aerospace Sciences*, Vol. 41, No. 7, 2005, pp. 515–557. doi:10.1016/j.paerosci.2005.09.002

[18] Yavuz, M. M., and Rockwell, D., "Control of Flow Structure on Delta Wing with Steady Trailing-Edge Blowing," *AIAA Journal*, Vol. 44, No. 3, March 2006, pp. 493–501. doi:10.2514/1.16444

[19] Gursul, I., Wang, Z., and Vardaki, E., "Review of Flow Control Mechanisms of Leading-Edge Vortices," *Progress in Aerospace Sciences*, Vol. 43, 2007, pp. 246–270. doi:10.1016/j.paerosci.2007.08.001

[20] Menke, M., and Gursul, I., "Unsteady Nature of Leading-Edge Vortices," *Physics of Fluids*, Vol. 9, No. 10, 1997, pp. 2960–2966. doi:10.1063/1.869407

[21] Atta, R., and Rockwell, D., "Hysteresis of Vortex Development and Breakdown on an Oscillating Delta Wing," *AIAA Journal*, Vol. 25, No. 11, 1987, pp. 1512–1513. doi:10.2514/3.9812

[22] Atta, R., and Rockwell, D., "Leading-Edge Vortices Due to Low Reynolds Number Flow Past a Pitching Delta Wing," *AIAA Journal*, Vol. 28, No. 6, 1990, pp. 995–1004. doi:10.2514/3.25156

[23] LeMay, S. P., Batill, S. M., and Nelson, R. C., "Vortex Dynamics on a Pitching Delta Wing," *Journal of Aircraft*, Vol. 27, No. 2, 1990, pp. 131–138. doi:10.2514/3.45908

[24] Greenwell, D. I., and Wood, N. J., "Some Observations on the Dynamic Response to Wing Motion of the Vortex Burst Phenomenon," *The Aeronautical Journal*, Vol. 98, No. 972, Feb. 1994, pp. 49–59.

[25] Gursul, I., "Review of Unsteady Vortex Flows over Slender Delta Wings," *Journal of Aircraft*, Vol. 42, No. 2, March–April 2005, pp. 299–319. doi:10.2514/1.5269

[26] Jiang, P., "Interaction of Thrust Vectoring Jets with Wing Vortical Flows," Ph.D. Thesis, Univ. of Bath, Bath, England, UK, 2009.

[27] Polhamus, E. C., "Predictions of Vortex-Lift Characteristics by a Leading-Edge Suction Analogy," *Journal of Aircraft*, Vol. 8, No. 4, April 1971, pp. 193–199. doi:10.2514/3.44254

[28] Gursul, I., Srinivas, S., and Batta, G., "Active Control of Vortex Breakdown over a Delta Wing," *AIAA Journal*, Vol. 33, No. 9, 1995, pp. 1743–1745. doi:10.2514/3.12721

[29] Thompson, S. A., Batill, S. M., and Nelson, R. C., "Separated Flowfield on a Slender Wing Undergoing Transient Pitching Motions," *Journal of Aircraft*, Vol. 28, No. 8, 1991, p. 489. doi:10.2514/3.46053

[30] Magness, C., Robinson, O., and Rockwell, D., "Laser-Scanning Particle Image Velocimetry Applied to a Delta-Wing in Transient Maneuver," *Experiments in Fluids*, Vol. 15, No. 3, 1993, pp. 159–167.

[31] Reisenthel, P. H., Xie, W., Gursul, I., and Bettencourt, M. T., "An Analysis of Fin Motion Induced Vortex Breakdown," AIAA Paper 99-0136, Jan. 1999.